PHYSICAL REVIEW C **81**, 041302(R) (2010)

Two-proton knockout from ^{32}Mg: Intruder amplitudes in ^{30}Ne and implications for the binding of ^{29,31}F

P. Fallon,[1] E. Rodriguez-Vieitez,[1,2] A. O. Macchiavelli,[1] A. Gade,[3,4] J. A. Tostevin,[5] P. Adrich,[3] D. Bazin,[3] M. Bowen,[3,4] C. M. Campbell,[3,4] R. M. Clark,[1] J. M. Cook,[3,4] M. Cromaz,[1] D. C. Dinca,[3,4] T. Glasmacher,[3,4] I. Y. Lee,[1] S. McDaniel,[3,4] W. F. Mueller,[3] S. G. Prussin,[2] A. Ratkiewicz,[3,4] K. Siwek,[3,4] J. R. Terry,[3,4] D. Weisshaar,[3] M. Wiedeking,[1] K. Yoneda,[3,4] B. A. Brown,[3,4] T. Otsuka,[6,7] and Y. Utsuno[8]

[1]*Nuclear Science Division, Lawrence Berkeley National Laboratory, Berkeley, California 94720, USA*
[2]*Department of Nuclear Engineering, University of California, Berkeley, California 94720, USA*
[3]*National Superconducting Cyclotron Laboratory, Michigan State University, East Lansing, Michigan 48824, USA*
[4]*Department of Physics and Astronomy, Michigan State University, East Lansing, Michigan 48824, USA*
[5]*Department of Physics, Faculty of Engineering and Physical Sciences, University of Surrey, Guildford, Surrey GU2 7XH, United Kingdom*
[6]*Department of Physics, University of Tokyo, Hongo, Bunkyo-ku, Tokyo, 113-0033, Japan*
[7]*RIKEN, Hirosawa, Wako-shi, Saitama 351-0198, Japan*
[8]*Japan Atomic Energy Agency, Tokai, Ibaraki 319-1195, Japan*

(Received 4 April 2009; published 5 April 2010)

γ-ray decays from excited states in ^{30}Ne and inclusive and exclusive cross sections were measured in the ^{9}Be(^{32}Mg,^{30}Ne + γ)X two-proton knockout reaction at incident beam energies of 99.7 and 86.7 MeV/nucleon. The measured cross section is suppressed compared to calculations and is indicative of a reduced overlap of initial and final state wave functions in ^{32}Mg and ^{30}Ne. We interpret this reduction as due to large $4p4h$ amplitudes present in the ^{30}Ne ground state wave function, but not ^{32}Mg. Such large intruder components are predicted to help stabilize the heavier fluorine isotopes against neutron emission.

DOI: 10.1103/PhysRevC.81.041302 PACS number(s): 23.20.Lv, 21.60.Cs, 25.60.Je, 27.30.+t

The region of nuclei close to the neutron dripline is important in nuclear synthesis, and is one where weak nucleon binding and changes in the neutron-proton ratio (N/Z) can dramatically affect the underlying shell structure and nuclear properties. While technical advances continue to extend the frontier of neutron-rich nuclei, many remain beyond experimental reach and it is necessary to rely on calculation. In this context, the near-dripline fluorine and neon nuclei, with proton numbers $Z = 9, 10$ and neutron number $N \sim 20$, provide a unique region accessible to experiment, where the effects of weak binding and increasing N/Z asymmetry coexist and can give rise to measurable effects. It is here, for example, that $N = 20$ ceases to be a "magic" shell closure [1] and a new shell gap emerges at $N = 16$. This is also where a dramatic jump in stability occurs between oxygen and fluorine, i.e., adding one proton extends the location of the dripline an extra six neutrons from $^{24}_{8}O_{16}$ to $^{31}_{9}F_{22}$.

The breakdown of the $N = 20$ shell gap is an example of nucleon-nucleon (spin-isospin, $T = 0$) interactions modifying single-particle energies and driving shell evolution [2] as well as deformation [3,4]. This gives rise to the well known "island of inversion" [5–8] around ^{32}Mg; where nuclear shapes switch from spherical to deformed due to the enhanced contribution from correlations generated by promoting neutron pairs across the reduced sd-fp ($N = 20$) shell gap. The enhanced stability of the most neutron-rich fluorine isotopes has also been linked [9] to a broken $N = 20$ shell and the increased contribution from correlations due to large fp-shell ("intruder") occupancy.

In this Rapid Communication we present data and calculations on $^{30}_{10}Ne_{20}$, which is situated close to the last known, possibly last bound, isotopes of neon (^{34}Ne) and fluorine (^{31}F) and is also within the island of inversion. The cross section for the ^{32}Mg two-proton knockout reaction is measured and is found to be suppressed compared to calculation, indicating larger than predicted structural changes between the initial ^{32}Mg ground state and ^{30}Ne final states. The cross-section data are used to estimate the neutron fp-shell occupation probabilities in ^{30}Ne. We discuss these results in the context of the $N = 20$ shell gap and enhanced stability of neutron-rich ^{29,31}F.

Data were taken in two experiments at the National Superconducting Cyclotron Laboratory at Michigan State University. In both experiments ^{32}Mg ions were produced by fragmenting a 140 MeV/nucleon ^{48}Ca beam on a 850 mg/cm^2 ^{9}Be production target. The A1900 fragment separator [10], operated with a 2% momentum acceptance, was used to select and transport the ^{32}Mg ions to the S800 [11] beamline where they underwent reactions on a second ^{9}Be target at the target position of the S800 spectrograph. In the first (second) experiment the ^{32}Mg secondary beam energy was 99.7 (86.7) MeV/nucleon incident on a 565 (376) mg/cm^2 ^{9}Be target. ^{30}Ne fragments were identified by momentum and energy loss measurements at the S800 focal plane, and by time of flight between the A1900 and S800 focal plane scintillators. γ rays from reactions on the secondary target were detected using SeGA (Segmented Germanium Array) [12], consisting of seventeen 32-fold segmented germanium detectors situated 20 cm from the target in two rings at 90° and 37° relative to the beam axis. In this configuration SeGA had ∼2% photopeak efficiency for a 1 MeV γ ray, measured with a ^{152}Eu calibration source. The segmentation allowed event-by-event Doppler

correction to the energy of γ rays emitted from the fast moving ($v \approx 0.4c$) nuclei. The γ-ray energy resolution after Doppler correction was ~3%, full-width at half-maximum, at 1 MeV.

The ^{9}Be(^{32}Mg,^{30}Ne + γ)X knockout reaction at ~100 MeV/nucleon involves the sudden removal of two protons from the already neutron-rich ^{32}Mg nucleus, and is expected to proceed as a direct reaction [13]. The alternative (indirect) mechanism would involve one-proton knockout to excited states lying above the first proton threshold (of 17.7 MeV) in ^{31}Na followed by proton evaporation, and is expected to be highly suppressed due to the low neutron threshold (3.78 MeV) of ^{31}Na. A formalism for calculating cross sections for such sudden, direct, two-nucleon removal reactions, that combines eikonal dynamics and shell model structure descriptions, is presented in Refs. [14,15]. There, and more recently in [16,17] for the associated momentum spectra of the two-nucleon removal reaction residues, it is shown that the reaction dynamics restricts these direct removal events to grazing collisions between the projectile and target. This defines a (near cylindrical) volume through the projectile surface in which the collision with the target samples the joint position and momentum amplitudes of the wave functions of the two removed nucleons [18]. The shell model then provides this two-nucleon amplitude information. In the present case they are used to provide the (two-nucleon) amplitudes for finding a proton pair in each total J^{π} configuration coupled to the ^{30}Ne(J^{π}) core in the ^{32}Mg(0^{+}) ground state.

Assessments of these model calculations have been carried out in the above references, Refs. [13,19] and elsewhere, using inclusive and exclusive data of reactions, at ~100 MeV/nucleon, on test-case, spherical *sd*-shell nuclei (remote from the island of inversion). Full *sd*-shell model calculations are well studied for such systems and are expected to be rather reliable. These analyses confirm the sensitivity of both the cross section and momentum distributions of reaction residues to the structure of the initial and final states, through the spatial proximity of the removed nucleons and their angular momentum coupling, as is encoded in the shell-model structure amplitudes. Residue momentum spectra, probably the most direct measure of the quality of the (direct) reaction dynamics description, show excellent quantitative agreement with the data available for the *sd*-shell test-case systems [16,17].

The γ-ray spectrum obtained in coincidence with ^{30}Ne is shown in Fig. 1, and is a sum of data from both experiments. A strong transition is seen at 792(4) keV and a weaker γ ray at 1443(11) keV. An analysis of the spectrum fluctuations indicates the "peak" at 1100 keV has a ~20% chance to be a random fluctuation and is not a strong candidate for a γ ray (the 1443 keV peak has only a $\sim 10^{-4}$% probability of being random). The 792 keV transition confirms the 791(26) keV peak reported in [20], where it is assigned to the decay of the first excited $J^{\pi} = 2^{+}_{1}$ state to the ground state. The new 1443(11) keV transition is assigned to the $4^{+} \rightarrow 2^{+}$ decay as discussed below.

Three shell model calculations of ^{30}Ne are shown in Fig. 1 corresponding to different active valence spaces and/or two-body nucleon-nucleon effective interactions as described in the caption. The main physical difference is that in calculation "a" the ^{30}Ne states have only *sd*-shell components and a

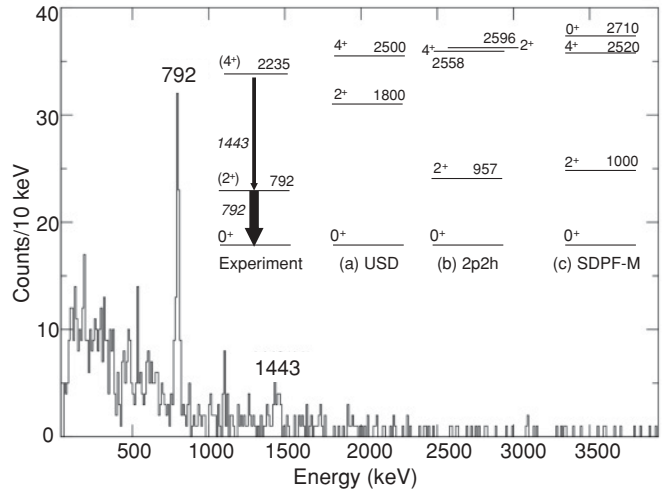

FIG. 1. Spectrum of γ rays in coincidence with ^{30}Ne. Insert: ^{30}Ne experimental levels and shell model calculated positive parity levels below the 3 MeV neutron separation energy. Calculation "a" involves only *sd*-shell ($0p0h$) configurations and uses the OXBASH [21] shell model code with the "universal-*sd*" (USD) effective interaction [22]. Calculation "b" uses the OXBASH code and WBMB interaction [8] with two neutrons occupying the *fp*-shell (two holes in the *sd*-shell). Calculation "c" uses the Monte Carlo shell model code and SDPF-M interaction [23], and allows *sd*-*fp* cross-shell excitations and mixed $0p0h$, $2p2h$, $4p2h$ configurations. The second 2^{+} in calculation "c" is located at 3.22 MeV.

spherical shape, while "b" and "c" include *sd*-*fp* cross-shell components and ^{30}Ne has a strong *prolate-deformed* shape. The number, n, of particles in the *fp* shell and the number of holes in the *sd* shell is denoted $npnh$. The relatively low energy for the 792 keV $2^{+} \rightarrow 0^{+}$ transition is consistent with a prolate deformation, $\beta_2 \sim 0.4$. Calculations "b" and "c", with *fp* shell components, reproduce a low 2^{+} energy, but overestimate its value. The ^{30}Ne (p, p') data [20] gave an electric quadrupole transition rate $B(E2 : 0^{+} \rightarrow 2^{+}) = 460(270)\ e^2\text{fm}^4$ also consistent with, albeit with large uncertainty, a deformed ^{30}Ne ground state. Our Monte Carlo shell model calculations with the SDPF-M interaction predict $B(E2 : 0^{+} \rightarrow 2^{+}) = 348\ e^2\text{fm}^4$.

We will make use of the direct nature of the ^{32}Mg-2p reaction to place the observed 1443 keV γ ray in the ^{30}Ne excitation scheme and derive values for neutron occupancies in ^{30}Ne. In ^{32}Mg the four valence protons occupy the strongly bound *sd* shell and predominantly the $d_{5/2}$ state. Two protons removed from a $(d_{5/2})^4$ configuration can couple to $J^{\pi} = 0^{+}, 2^{+}, 4^{+}$, and thus these are the final state spins directly populated in ^{30}Ne. Monte Carlo shell model calculations have been successful in describing energies and transition rates in and around the island of inversion due to their ability to handle the very large model space needed to include configurations with cross-shell components. This is the first use (test) of Monte Carlo shell model wave functions in reaction calculations.

An inclusive ^{9}Be(^{32}Mg,^{30}Ne) reaction cross section of $\sigma = 0.22(4)$ mb was derived from the number of ^{30}Ne ions detected in the S800 focal plane, relative to the number

TABLE I. Two proton removal cross sections (mb). Experimantal values for ^{28}Mg are from [13].

	^{32}Mg-2p				^{28}Mg-2p	
	Expt	SDPF-M	2p2h	USD	Expt	USD
0_1^+	0.13(3)	0.64	0.63	1.18	0.70(15)	1.19
0_2^+		0.03				
2_1^+	0.05(1)	0.08	0.05	0.77	0.09(15)	0.32
2_2^+		0.09	0.11	0.05	0.15(9)	0.45
4_1^+	0.04(1)	0.38	0.31	1.03	0.58(9)	1.02
Inclusive	0.22(4)	1.22	1.09	2.98	1.50(10)	2.98

of incoming ^{32}Mg ions and target nuclei. Corrections were applied for the data acquisition dead time, the S800 focal plane acceptance for ^{30}Ne residues, and detector efficiencies. Measured cross sections to ^{30}Ne states are given in Table I together with results from three calculations using the two-nucleon amplitudes derived from the calculations in Fig. 1. The measured value for a direct ground-state population of ∼60% was obtained assuming the 792 keV ($2_1^+ \rightarrow 0_1^+$) transition collects all the excited state flux, as expected in a deformed even-even nucleus. This is a robust quantity independent of unobserved higher lying transitions. This value is reproduced by all calculations and is substantially larger than the ∼25% value expected if the protons were uncorrelated [18], reflecting the enhanced spatial correlations associated with time-reversed $J = 0^+$ pairs.

The 1443 keV transition is placed in cascade with the 792 keV transition and could correspond to the decay from either of the $J = 4_1^+, 2_2^+, 0_2^+$ states predicted around 2.5–3.0 MeV (Fig. 1). While it is not possible to use excitation energies to distinguish between these states, calculations show that their direct population cross section exhibits a strong spin-dependence (Table I and Fig. 2) and provides a way to distinguish them. Direct population of the 4_1^+ state has a larger cross section than either the $2_{1,2}^+$ state, and consequently the majority of the 75 counts observed in the 792 keV peak in Fig. 1 would come from feeding via the 4_1 state. This means, according to the calculation, that a ∼1500 keV $4_1^+ \rightarrow 2_1^+$ transition should be visible in Fig. 1 with ∼30(5) counts. The observed 1443 keV transition has 20(5) counts and is thereby assigned to the $4_1^+ \rightarrow 2_1^+$ decay. This characteristic population pattern is also predicted and observed in the analogous ^{28}Mg-2p reaction [13,15] (Table I), following 2p removal from a $(d_{5/2})^4$ configuration.

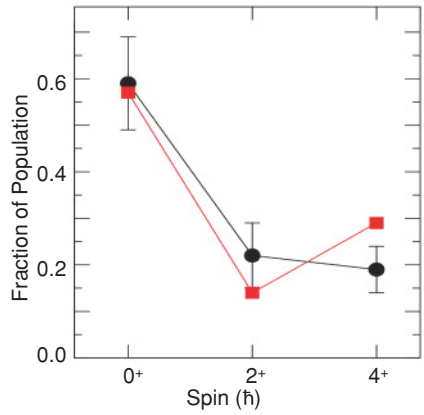

FIG. 2. (Color online) Calculated (squares) and experimental (circles) fractional population of spin J = 0^+, 2^+, 4^+ states in ^{30}Ne after two-proton knockout from ^{32}Mg. Calculated values use the SDPF-M two-nucleon amplitudes. The calculated 2^+ value is a sum of the 2_1^+ and 2_2^+ cross sections.

We now return to the magnitude of the measured inclusive two-proton removal cross section and its implications for the neutron fp intruder structure in ^{30}Ne. For all shell model wave functions used here the calculated cross sections exceed the measured values by a factor of 4 or more. The USD wave functions give larger values, but these are known to be unrealistic for the nuclei of interest here. To the extent that structural changes between initial and final states are correctly tracked by the shell model, such changes would already be included in the two-nucleon amplitudes and reflected in the calculated cross section. The observed reduction in the measured cross sections suggests the shell model is not able to track these changes adequately. It was shown in [24], for two-proton removal from ^{38}Si, the initial to final state overlaps and the two-proton removal cross section can be reduced due to structural changes in the dominant neutron configurations.

As discussed earlier, the calculated two-nucleon removal cross sections and data have been tested quantitatively for several test case, 0p0h, spherical nuclei [15,19]. The result was that theoretical calculations overestimated the data by a factor of 2, as shown in Fig. 3 for the test case examples: ^{26}Si, ^{30}S, ^{34}Ar, ^{28}Mg, and ^{54}Ti. For these nuclei $\sigma_{ex} = R_s(2N) \times \sigma_{th}$ and the two-nucleon suppression factor $R_s(2N)$ took the value 0.5. This reduction of cross-section yield [25],

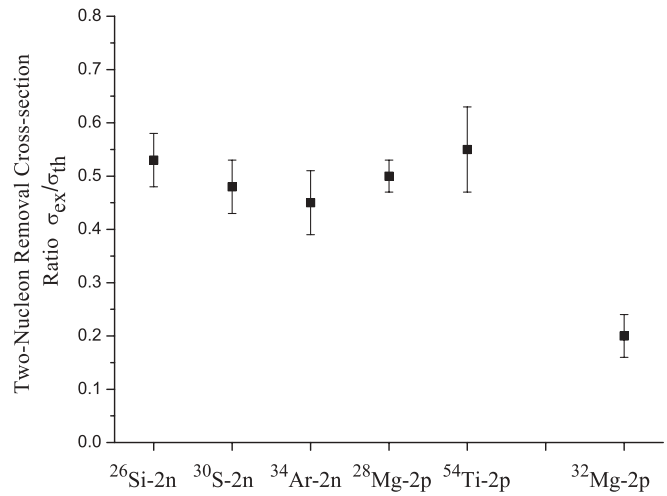

FIG. 3. Two-nucleon removal cross-section ratios, σ_{ex}/σ_{th}, derived from inclusive cross section measurements and calculations (note ^{54}Ti-2p is for $0^+ \rightarrow 0^+$). The data for the ^{26}Si-2n, ^{30}S-2n, ^{34}Ar-2n, ^{28}Mg-2p, and ^{54}Ti-2p two-nucleon removal reactions correspond to the test-case nuclei discussed in the text and are taken from [15,19], and references therein. The σ_{ex}/σ_{th} value for the ^{32}Mg-2p $0^+ \rightarrow 0^+$ reaction is also included and shows an additional suppression, discussed in the text.

similar to that observed in both electron- and nuclear-induced one-nucleon removal, is interpreted as due to the use of a small, truncated shell model space. For the ^{32}Mg two-proton removal reaction, also shown in Fig. 3, σ_{ex}/σ_{th} is reduced even further. We express the ^{32}Mg-$2p$ experimental cross section as $\sigma_{ex} = [P_{if}\, R_s(2N)] \times \sigma_{th}$, where P_{if} is now included to account for the reduction of the square of the initial to final neutron state overlaps, i.e., changes beyond those present in the shell model calculations. We associate P_{if} with the neutron overlap because the proton configurations in ^{32}Mg and ^{30}Ne are well-bound, sd-shell states and the shell model is assumed to provide a reliable description of these. The fact the observed $\sigma(J)$ follow the trend expected for $(d_{5/2})^4 - 2p$ removal, Fig. 2, supports our assertion that the overall scaling is associated with changes of neutron configurations.

From the measured ^{32}Mg-$2p$ ($0^+_1 \rightarrow 0^+_1$) cross section, $\sigma_{ex} = 0.13(3)$ mb, and the corresponding $\sigma_{th} = 0.64$ mb (SDPF-M in Table I) we obtain a total suppression $[P_{if}\, R_s(2N)] = 0.20(4)$ and, for $R_s(2N) = 0.5$, a value $P_{if} \approx 0.4$. Similar numbers are obtained using the inclusive cross sections. This value of P_{if} can now be used to estimate the ^{30}Ne neutron intruder configuration. We make the simplifying assumption, $|\Phi\rangle = |\phi_\pi\rangle|\phi_\nu\rangle$, and write the neutron wave function as a combination of $np$$n$h excitations: $|\phi_\nu\rangle = \alpha|0p0h\rangle + \beta|2p2h\rangle + \gamma|4p4h\rangle$. One-neutron knockout data [26] indicate ^{32}Mg has a neutron intruder occupancy $n(fp) \sim 2$, and all evidence to date points to both ^{32}Mg and ^{30}Ne ground state wave functions being primarily $np$$n$h ($n \geqslant 2$) with little $0p0h$. The mismatch in σ_{ex} and σ_{th} arising from the neutron overlap function is then mainly due to differences in the $2p2h$ and $4p4h$ neutron components. With $P_{if} \approx 0.4$ obtained above and assuming the ^{32}Mg ground state is dominated by neutron $2p2h$ components ($\geqslant$90%, as reported in [26]), we estimate the ^{30}Ne ground state to have approximately equal amounts of $2p2h$ and $4p4h$ components, both $\sim$50%. This gives an average ^{30}Ne fp-shell neutron intruder occupancy $n(fp) \sim 3$; a significant increase compared with ^{32}Mg.

The large ^{30}Ne intruder ($4p4h$) content and difference between the ^{30}Ne and ^{32}Mg neutron configurations deduced in this measurement have important consequences. First, they indicate an increasing erosion of the $N = 20$ shell gap through the island of inversion (^{32}Mg $\rightarrow$ ^{30}Ne) [23]. Second, such large intruder amplitudes are predicted (needed) [9] to stabilize the heavier fluorine isotopes, ^{29,31}F, against neutron emission; due to the increased contribution from the correlation energy (deformation, pairing) gained from promoting more neutrons to the fp-shell and opening the valence space.

Table II shows calculated ground-state neutron intruder occupation probabilities for ^{32}Mg, ^{30}Ne, and ^{29,31}F. The SDPF-M interaction used here provides a good description of many nuclei (both ground state properties and low lying spectra) from ^{40}Ca to ^{32}Mg. However, while it predicts ^{29}F to be particle bound it does not bind ^{31}F [9]. Refinement of this interaction to describe the intruder admixture ($\sim$50% $4p4h$) at ^{30}Ne is a challenge. Extending this shell model space to include the $2p_{1/2}$ and $1f_{5/2}$ levels is an extension that could generate higher neutron intruder components in ^{30}Ne and ^{29,31}F. However, these nuclei are also located close to the dripline and it is intriguing to explore other effects (e.g., weak binding) that may effectively increase the correlation energy and act locally.

TABLE II. Ground state neutron $0p0h$, $2p2h$, $4p4h$ probabilities (%) for ^{32}Mg, ^{30}Ne, ^{29,31}F calculated using the SDPF-M interaction in the Monte Carlo shell model code.

	$0p2h$	$2p2h$	$4p4h$
^{32}Mg	4.7	82.5	12.7
^{30}Ne	3.9	74.1	22.0
^{29}F	8.0	62.7	28.8
^{31}F	15.6	65.9	18.4

Weak binding can influence the level spacing due to the changing centrifugal barriers with orbital angular momentum (l) values [27]. The wave function for a low-l orbital can extend appreciably beyond the average nuclear radius (halo effect) causing its energy to be less sensitive to changes in the radius (or A), thereby altering the density of states near the Fermi surface that could then favor multiple particle-hole excitations. These effects are not accounted for in shell model calculations due to the use of harmonic oscillator wave functions. In the Monte Carlo shell model calculation of Ref. [9] the effect of a neutron $p_{3/2}$ "halo" was simulated by a 350 keV lowering of the $p_{3/2}$ state. The result was that ^{31}F became bound. Enhanced ^{30}Ne $4p4h$ amplitudes can also be interpreted in a Nilsson model [28] as a consequence of larger deformation compared with ^{32}Mg. It was pointed out [27] that (near) degenerate fp levels will favor deformation.

While a fully quantitative evaluation of the effects of extending the shell model space and of weak binding on the shell model wave functions and overlaps is beyond the scope of this work, we can simulate (in part) their effects through an ad hoc lowering of the $1f_{7/2}$ and $2p_{3/2}$ single-particle energies, each by 800 keV. This reduces the $N = 20$ gap and increases the ^{30}Ne, ^{29}F, and ^{31}F $4p4h$ amplitudes to 49%, 51%, and 36%, respectively, and so simulates the consequences of such intruder components on the properties of ^{30}Ne and ^{29,31}F. The results are (i) the calculated ^{30}Ne 2^+_1 and 4^+_1 energies are lowered to 830 keV and 2380 keV, closer to experiment, (ii) the ^{30}Ne $B(E2 : 0^+_1 \rightarrow 2^+_1)$ increases from 348 to 401 e^2fm^4, and (iii) ^{31}F becomes bound as experiment requires.

To conclude, the ^{9}Be(^{32}Mg,^{30}Ne) reaction at intermediate energies was used to investigate the structure of the near dripline nucleus ^{30}Ne through a combination of spectroscopy and reaction measurements and large-scale shell model calculations. The two-proton removal cross section was found to be suppressed compared with calculation, indicating a reduced overlap between the initial ^{30}Ne and final ^{32}Mg state wave functions. We interpret this reduction in terms of an increased occupancy of neutron $4p4h$ intruder configurations in ^{30}Ne, compared with ^{32}Mg. This result is relevant to the binding of ^{29}F and ^{31}F, where large intruder amplitudes are predicted to help stabilize the heavier fluorine isotopes. It is an interesting possibility that weak binding effects could play a role in producing such enhanced intruder amplitudes and defining the fluorine dripline.

We gratefully acknowledge the help of the NSCL operations staff. We thank Prof. Hamamoto for illuminating discussions. This work was supported by the DOE Office of Nuclear Physics under Contract No. DE-AC02-05CH11231, the National Science Foundation under Grant Nos. PHY-0606007 and PHY-0758099, and by the UK Science and Technology Facilities Council under Grant Nos. ST/F012012 and EP/D003628.

[1] O. Sorlin and M.-G. Porguet, Prog. Part. Nucl. Phys. **61**, 602 (2008).
[2] T. Otsuka, T. Suzuki, R. Fujimoto, H. Grawe, and Y. Akaishi, Phys. Rev. Lett. **95**, 232502 (2005).
[3] A. De Shalit and M. Goldhaber, Phys. Rev. **92**, 1211 (1953).
[4] P. Federman and S. Pittel, Phys. Rev. C **20**, 820 (1979).
[5] C. Thibault *et al.*, Phys. Rev. C **12**, 644 (1975).
[6] C. Detraz *et al.*, Phys. Rev. C **18**, 164 (1979).
[7] X. Campi *et al.*, Nucl. Phys. A **251**, 193 (1975).
[8] E. K. Warburton, J. A. Becker, and B. A. Brown, Phys. Rev. C **41**, 1147 (1990).
[9] Y. Utsuno, T. Otsuka, T. Mizusaki, and M. Honma, Phys. Rev. C **64**, 011301(R) (2001).
[10] D. J. Morrissey *et al.*, Nucl. Instrum. Methods B **204**, 90 (2003).
[11] D. Bazin *et al.*, Nucl. Instrum. Methods B **204**, 629 (2003).
[12] W. F. Mueller *et al.*, Nucl. Instrum. Methods A **466**, 492 (2001).
[13] D. Bazin *et al.*, Phys. Rev. Lett. **91**, 012501 (2003).
[14] J. A. Tostevin, G. Podolyak, B. A. Brown, and P. G. Hansen, Phys. Rev. C **70**, 064602 (2004).
[15] J. A. Tostevin and B. A. Brown, Phys. Rev. C **74**, 064604 (2006).
[16] E. C. Simpson, J. A. Tostevin, D. Bazin, B. A. Brown, and A. Gade, Phys. Rev. Lett. **102**, 132502 (2009).
[17] E. C. Simpson, J. A. Tostevin, D. Bazin, and A. Gade, Phys. Rev. C **79**, 064621 (2009).
[18] J. A. Tostevin, J. Phys. Conf. Ser. **49**, 21 (2006).
[19] K. Yoneda *et al.*, Phys. Rev. C **74**, 021303(R) (2006).
[20] Y. Yanagisawa *et al.*, Phys. Lett. B **566**, 84 (2003).
[21] B. A. Brown *et al.*, MSU-NSCL Report No. 524.
[22] B. A. Brown and B. H. Wildenthal, Annu. Rev. Nucl. Part. Sci. **38**, 29 (1988).
[23] Y. Utsuno, T. Otsuka, T. Mizusaki, and M. Honma, Phys. Rev. C **60**, 054315 (1999).
[24] A. Gade *et al.*, Phys. Rev. Lett. **99**, 072502 (2007).
[25] B. A. Brown, P. G Hansen, B. M Sherrill, and J. A Tostevin, Phys. Rev. C **65**, 061601(R) (2002).
[26] J. R. Terry *et al.*, Phys. Rev. C **77**, 014316 (2008).
[27] I. Hamamoto, Phys. Rev. C **76**, 054319 (2007).
[28] A. Bohr and B. R. Mottelson, *Nuclear Structure* (World Scientific Publishing Co. Pte. Ltd., Singapore, 1998), Vol. 2, Chap. 5.